SUBMITTED TO THE ASTROPHYSICAL JOURNAL
Preprint typeset using LaTeX style emulateapj v. 10/09/06

LIMITS OF BINARIES THAT CAN BE CHARACTERIZED BY GRAVITATIONAL MICROLENSING

DOEON KIM[1], YOON-HYUN RYU[2], BYEONG-GON PARK[3], HEON-YOUNG CHANG[2], KYU-HA HWANG[1], SUN-JU CHUNG[3], CHUNG-UK LEE[3], AND CHEONGHO HAN[1,4]

Submitted to The Astrophysical Journal

ABSTRACT

Due to the high efficiency of planet detections, current microlensing planet searches focus on high-magnification events. High-magnification events are sensitive to remote binary companions as well and thus a sample of wide-separation binaries are expected to be collected as a byproduct. In this paper, we show that characterizing binaries for a portion of this sample will be difficult due to the degeneracy of the binary-lensing parameters. This degeneracy arises because the perturbation induced by the binary companion is well approximated by the Chang-Refsdal lensing for binaries with separations greater than a certain limit. For binaries composed of equal mass lenses, we find that the lens binarity can be noticed up to the separations of ~ 60 times of the Einstein radius corresponding to the mass of each lens. Among these binaries, however, we find that the lensing parameters can be determined only for a portion of binaries with separations less than ~ 20 times of the Einstein radius.

Subject headings: gravitational lensing

1. INTRODUCTION

Searches for extrasolar planets by using microlensing are being carried out by observing stars located toward the Galactic bulge field. The lensing signal of a planet is a short-duration perturbation to the smooth standard light curve of the primary-induced lensing event occurring on a background star (Mao & Paczyński 1991; Gould & Loeb 1992). For the detections of the short-duration planetary lensing signals, these searches are using a combination of survey and follow-up observations, where the survey observations (e.g., OGLE, Udalski (2003); MOA, Bond et al. (2002a)) aim to maximize the lensing event rate by monitoring a large area of sky and the follow-up observations (e.g., PLANET, Albrow et al. (2001); MicroFUN, Dong et al. (2006)) intensively monitor the events alerted by the survey observations. However, the limited number of telescopes restricts the number of events that can be followed at any given time and thus priority is given to those events that will maximize the planetary detection probability. Currently, the highest priority is given to high-magnification events because the source trajectories of these events always pass close to the perturbation region around the planet-induced caustic located near the primary lens (Griest & Safizadeh 1998). In addition, follow-up observations can be prepared for these events because the perturbation typically occurs near the peak of the event, which can be predicted from the data on the rising part of the event light curve. As a result, six (OGLE-2005-BLG-071Lb, OGLE-2005-BLG-169Lb, OGLE-2006-BLG-109Lb,c, MOA-2007-BLG-400b, MOA-2007-BLG-192) of the eight reported microlensing planets were detected through the channel of high-magnification events (Bond et al. 2004; Udalski et al. 2005; Beaulieu et al. 2006; Gould et al. 2006; Gaudi et al. 2008; Dong et al. 2008; Bennett et al. 2008).

In addition to planets, high-magnification events are sensitive to wide-separation binary companions as well. Similar to the planetary case, the companion of a wide-separation binary induces a small caustic close to the primary lens and thus can produce a short-duration perturbation near the peak of a high-magnification event. Due to the different nature of the companions, however, the perturbations induced by a wide-separation binary companion and a planet can be distinguished (Albrow et al. 2002; Han & Gaudi 2008). Therefore, under the current planetary lensing strategy focusing on high-magnification events, a considerable number of wide-separation binaries are expected to be detected as a byproduct and this sample might provide useful information about the physical distribution of binaries.

Unlike this expectation, however, we find that characterizing binaries for a significant portion of the binary lens sample will be difficult due to the degeneracy of the binary-lensing parameters. This degeneracy arises because the perturbation induced by the binary companion is well approximated by the Chang-Refsdal lensing (hereafter C-R lensing) for binaries with separations greater than a certain value. The C-R lensing represents single-mass lensing superposed on a uniform background shear. For a wide-separation binary, the shear results from the combination of the binary-lens parameters and thus the individual parameters cannot be separately determined.

The paper is organized as follows. In § 2, we briefly describe the properties of binary and C-R lensing. In § 3, we demonstrate the proximity between the binary and C-R lensing for binaries with separations beyond a certain limit. We then set the range in the binary-lensing parameter space where the degeneracy of binary-lensing parameters occurs. We discuss the meaning of this degeneracy in the studies of binaries by using microlensing. We summarize the results and conclude in § 4.

2. LENSING PROPERTIES

If a source is lensed by a single point mass, the lens mapping from the lens plane to the source plane is expressed by the lens equation

$$\zeta = z - \frac{1}{\bar{z}}, \tag{1}$$

[1] Department of Physics, Institute for Basic Science Research, Chungbuk National University, Chongju 361-763, Korea
[2] Department of Astronomy and Atmospheric Sciences, Kyungpook National University, Daegu 702-701, Korea
[3] Korea Astronomy and Space Science Institute, Hwaam-Dong, Yuseong-Gu, Daejeon 305-348, Korea
[4] corresponding author

where $\zeta = \xi + i\eta$ and $z = x + iy$ are the locations of the source and the lens in complex notations, respectively, and $\bar{z}$ denotes the complex conjugates of z. Here all angles are normalized by the angular Einstein radius of the lens, which is related to the physical parameters of the lens by

$$\theta_{\rm E} = \left(\frac{4GM}{c^2}\right)^{1/2}\left(\frac{1}{D_L}-\frac{1}{D_S}\right)^{1/2}, \qquad (2)$$

where M is the mass of the lens and D_L and D_S are the distances to the lens and source, respectively. Solving the lens equation results in two solutions of the image position. The lensing process conserves the source surface brightness and thus the magnifications of the individual images correspond to the area ratios between the images and source. Mathematically, this is obtained by solving the Jacobian of the mapping equation evaluated at the image position, i.e.,

$$A_i = \left|\left(1-\frac{\partial\zeta}{\partial\bar{z}}\overline{\frac{\partial\zeta}{\partial\bar{z}}}\right)^{-1}_{z=z_i}\right|. \qquad (3)$$

Then, the total magnification corresponds to the sum of the individual images, i.e., $A = \sum_i A_i$, and this results in

$$A = \frac{u^2+2}{u(u^2+4)^{1/2}}, \qquad (4)$$

where $u = |\zeta|$ represents the normalized lens-source separation. For a rectilinear motion, the lens-source separation is related to the lensing parameters of the Einstein time scale $t_{\rm E}$, the closest lens-source separation u_0, and the time at the moment t_0 by

$$u = \left[u_0^2+\left(\frac{t-t_0}{t_{\rm E}}\right)^2\right]^{1/2}. \qquad (5)$$

The light curve of a single-lensing event is characterized by a smooth and symmetric shape (Paczyński 1986).

If a source is lensed by a binary lens, on the other hand, the mapping equation is expressed as (Witt 1990)

$$\zeta = z - \frac{m_1/M}{\bar{z}-\bar{z}_{L,1}} - \frac{m_2/M}{\bar{z}-\bar{z}_{L,2}}, \qquad (6)$$

where $z_{L,1} = x_{L,1} + iy_{L,1}$ and $z_{L,2} = x_{L,2} + iy_{L,2}$ are the positions of the lens components, m_1 and m_2 are their masses, and $M = m_1 + m_2$ is the total mass of the binary. One important characteristic of binary lensing that differentiates from single lensing is the formation of caustics, which represent source positions at which the magnification of a point source becomes infinite. The set of caustics form closed curves, each of which is composed of concave curves (fold caustic) that meet at points (cusps). Binary lenses can have one, two, or three closed caustic curves. If the two masses are separated by approximately an Einstein radius, then there is a single six-cusp caustic. If the masses are much closer than an Einstein ring, there is a central four-cusp caustic and two outlying three-cusp caustics. If they are separated by much more than an Einstein ring (wide-separation binary), then there are two four-cusp caustics, where each of the caustics is associated with each member of the binary. In addition to the parameters of single lensing, modelling a binary-lensing event requires two additional lensing parameters of the separation $s = |z_{L,1} - z_{L,2}|$ and the mass ratio $q = m_2/m_1$ between the lens components.

The Chang-Refsdal lensing represents single lensing superposed on a uniform background shear (Chang & Refsdal 1979, 1984). The lens equation for the C-R lensing is represented by

$$\zeta = z - \frac{1}{\bar{z}} + \gamma\bar{z}, \qquad (7)$$

where γ is the shear. The shear induces a single set of caustics, which form around the lens. The caustic has a shape of a hypocycloid with four cusps. Its size as measured by the separation between two confronting cusps are related to the shear by

$$\Delta\zeta_c = 4\gamma. \qquad (8)$$

In the limiting case of a binary lens where the binary separation is much larger than the Einstein radius ($s \gg 1$), the lensing properties in the vicinity of each of the binary lenses is well described by that of the C-R lensing (Dominik 1999). The shear exerted by the companion is related to the binary parameters by

$$\gamma \sim \frac{q}{\hat{s}^2}; \qquad \hat{s} = (1+q)^{1/2}s, \qquad (9)$$

where $\hat{s}$ is the binary separation normalized by the Einstein radius corresponding to the mass of the lens close to which the caustic is located. The shear decreases as $1/\hat{s}^2$ and thus the caustics of a wide-separation binary lens shrink rapidly as the binary separation increases. In the limiting case where $\hat{s} \to \infty$, the shear and the caustics vanish and the individual lens components behave as if they are two independent single lenses. The positions of the lens components effectively working as single lenses, effective lens position $z_{L,eff}$, are slightly shifted from their original positions with an offset (Di Stefano & Mao 1996)

$$\Delta z_L = z_L - z_{L,eff} \sim -\frac{q}{\hat{s}}\frac{z_{L,2}-z_{L,1}}{|z_{L,2}-z_{L,1}|}. \qquad (10)$$

3. DEGENERACY

The fact that the lensing behavior of a wide-separation binary in the region close to each lens component is well described by the C-R lensing implies that although lens binarity can be noticed from the perturbation to the light curve of a high-magnification event, it may be difficult to determine the binary-lensing parameters from the analysis of the perturbation. This is because the C-R lensing is described by a single parameter of γ, which results from the combination of the two binary-lensing parameters of s and q.

Then, naturally rising questions are (1) how serious this degeneracy is and (2) in which region of the binary-lensing parameter space this degeneracy occurs. To answer these questions, we construct two sets of perturbation pattern maps as a function of the source position in the central region of a component of binary lenses with various separations and mass ratios. In the first set, we construct the maps of the fractional magnification residual from that of single lensing, i.e.,

$$\epsilon_s = \frac{A-A_s}{A_s}, \qquad (11)$$

where A and A_s are the magnifications of binary and single lensing without the companion, respectively. In the second set, we construct the maps of the residual from that of C-R lensing, i.e.,

$$\epsilon_{\rm C-R} = \frac{A-A_{\rm C-R}}{A_{\rm C-R}}, \qquad (12)$$

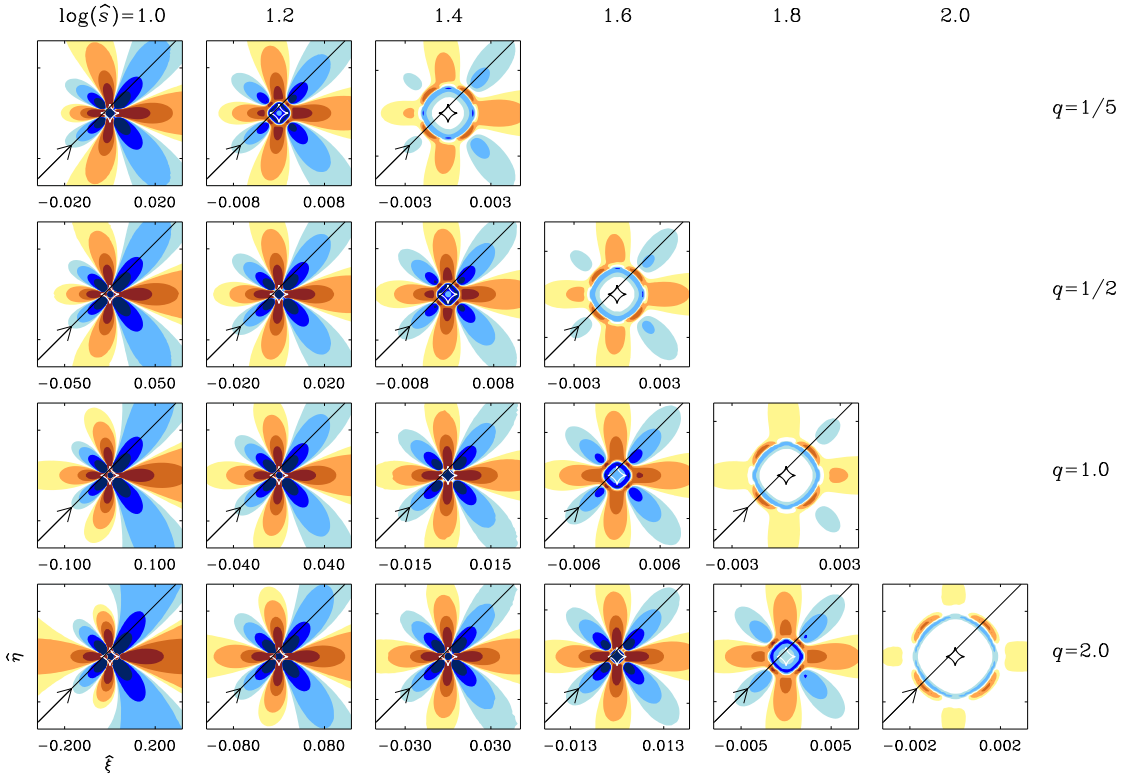

FIG. 1.— Maps of the fractional magnification residual from that of single lensing as a function of the source position in the central region of a component of binary lenses with various separations and mass ratios. All lengths are scaled by the Einstein radius corresponding to the mass of the binary component around which the map is constructed (primary). The coordinates are centered at the effective position of the primary lens (see the definition of the 'effective lens position' in the text of § 2). The width of each map corresponds to 8 times of the width of the caustic. In each map, the regions with blue and brown-tone colors represent the areas where the binary-lensing magnification is lower and higher than the single-lensing magnification, respectively. For each tone, the color changes into darker scales when the residual is $|\epsilon| \geq 1\%$, 2%, 5%, and 10%, respectively. The straight lines with arrows represent the source trajectories and the light curves of the resulting events are presented in the corresponding panels of Fig. 3. We note that maps are not presented if the perturbation from single lensing is severely washed out by the finite-source effect and thus the magnification pattern of a binary-lensing case is difficult to be distinguished from that of a single-lensing case.

where $A_{\rm C-R}$ is the magnification obtained from C-R lensing by approximating the shear exerted by the companion as $\gamma = q/\hat{s}^2$.

Figure 1 and 2 show the two sets of maps. In each map, the coordinates are centered at the effective position of a binary component. The width of each map is set such that it corresponds to 8 times of the width of the C-R lensing caustic computed by equations (8) and (9). The separation and the mass ratio of the binary for each map are marked at the top and on the right side of the panel, respectively. The mass ratio is such that $q < 1.0$ when the companion is less massive than the lens component around which the map is constructed and vice versa. In each map, the regions with blue and brown-tone colors represent the areas where the binary-lensing magnification is lower and higher than the single or C-R lensing magnification, respectively. For each tone, the color changes into darker scales when the residual is $|\epsilon| \geq 1\%$, 2%, 5%, and 10%, respectively. Figure 3 shows light curves of events resulting from the source trajectories marked in Figure 1. In the upper part of each panel, there are three curves: blue curve for single lensing, red curve for C-R lensing, and black curve for binary lensing. The lower part shows the fractional residuals from the single-lensing magnification (blue curve) and the C-R lensing approximation (red curve).

The caustic induced by a wide-separation binary is small and thus perturbations induced by the caustic are vulnerable to finite-source effect. The finite-source effect is parameterized by the ratio of the source radius $r_\star$ to the Einstein radius. For a lensing event toward the Galactic bulge field, this ratio is scaled by the physical parameters of the lens by

$$\rho_\star = 9 \times 10^{-4} \left(\frac{r_\star}{R_\odot}\right) \left[\left(\frac{m_1}{0.3\,M_\odot}\right)\left(\frac{D_L}{6\ {\rm kpc}}\right)\left(1-\frac{D_L}{D_S}\right)\right]^{-1/2}. \quad (13)$$

Then, the magnification affected by the finite-source effect becomes

$$A = \frac{\int_0^{\rho_\star} I(r) A_p(|\mathbf{r}-\mathbf{r}_L|) r dr}{\int_0^{\rho_\star} I(r) r dr}, \quad (14)$$

where $\mathbf{r}_L$ is the displacement vector of the source center with respect to the lens, $\mathbf{r}$ is the vector to a position on the source star surface with respect to the center of the source star, $I(r)$ represents the source brightness profile, and A_p is the point-source magnification. We consider the finite-source effect by assuming that the source star has a uniform disk with a radius equivalent to the Sun and the physical parameters of the lens system are $m_1 = 0.3\ M_\odot$, $D_L = 6$ kpc, and $D_S = 8$ kpc by adopting the values of a typical event being detected toward Galactic bulge field. This results in $\rho_\star = 1.8 \times 10^{-3}$. In Figure 1 – 3, we do not present maps and light curves if the perturbation from single lensing is severely washed out by the finite-source effect and thus the magnification pattern of a binary-lensing case is difficult to be distinguished from that of a single-lensing case.

The residual map from single lensing shows that although

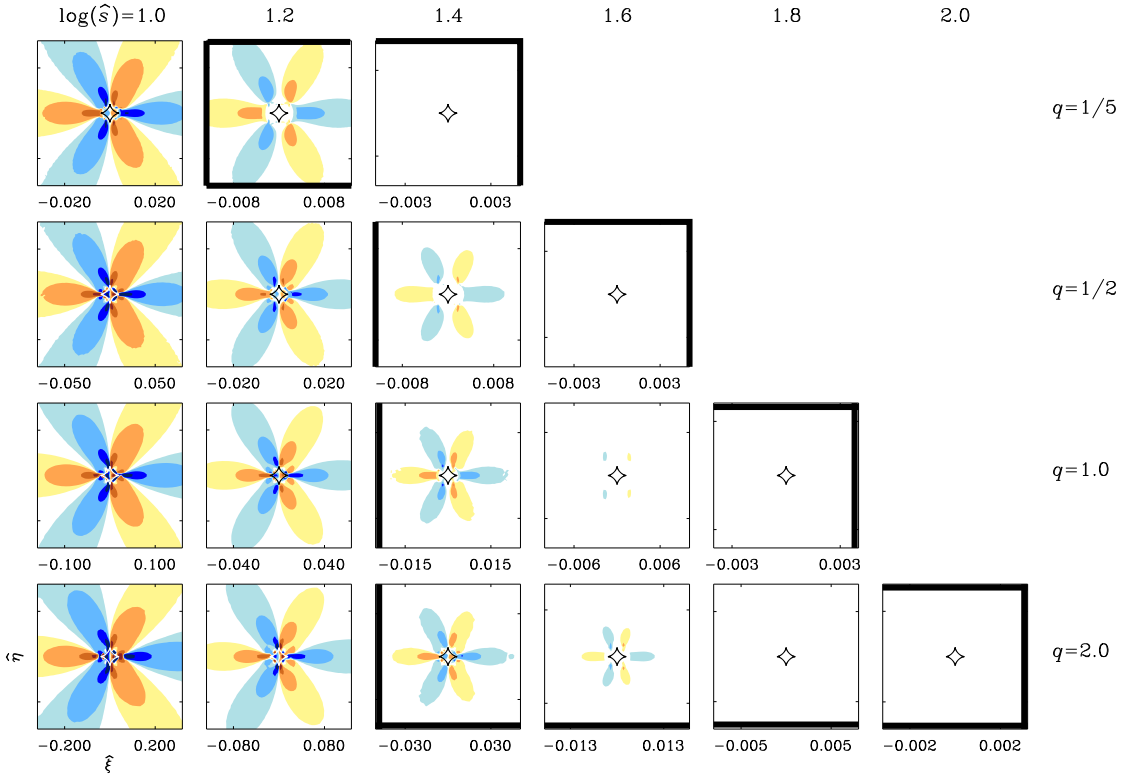

FIG. 2.— Same as Fig. 1 except that the magnification residual is from that of C-R lensing. The panels blocked by thick lines represent the cases where the binary signal can be detected, but characterization of the binary is difficult due to the degeneracy of the binary-lensing parameters.

the perturbation becomes weaker as the distance to the companion increases, it lasts for a considerable distance. The maximum distance for the detection of the companion signal depends on the companion/primary mass ratio and the observational precision. By adopting a threshold residual of $\epsilon_s = 5\%$, we find that companions can be detected up to the separations of $\hat{s} \sim 31$, 50, 63, and 100 for binary companions with mass ratios of $q = 1/5$, 1/2, 1.0, and 2.0, respectively. Considering that the physical radius of the Einstein ring is $r_{\rm E} \sim 1.9$, AU, these limits correspond to the physical separations of $d \sim 59$, 95, 120, and 190 AU, respectively, implying that high-magnification events provide an efficient channel to detect wide-separation binaries.

However, the condition for detection is different from the condition for characterization. The condition for binary characterization depends on various factors such as real experimental data, photometric errors, sampling rate, observation duration, and telescopes performance. Therefore, it is not easy to define a single observable that can be used for an indicator to judge the characterizability of binary-lens events. However, if a light curve significantly deviates from C-R lensing approximation, it would be possible to determine the binary-lensing parameters. The photometric error achieved by the current follow-up observations reaches down to $\sim 1-2\%$ level for high-magnification events (Gould 2008, private communication). We therefore set the condition for binary characterization such that light curves should be distinguished from the C-R lensing approximation with $\epsilon_{\rm C-R} \geq 5\%$. With this criterion, we find that the upper limits of binary separation for characterization are $\hat{s} \sim 13$, 20, 22, and 25 for binary companions with mass ratios of $q = 1/5$, 1/2, 1.0, and 2.0, respectively. From the comparison of the limits for detection, the ranges of binary separation for characterization are substantially narrower than the ranges for detection. This implies that for a significant fraction of events for which signals of wide-separation binary companions are detected, it will be difficult to characterize the properties of the binary by determining the lensing parameters. In Figure 2, we mark this region of degeneracy by blocking the panels with thick solid lines. We also list the detection and degeneracy regions in Table 1.

TABLE 1
DETECTION AND DEGENERACY ZONES

mass ratio	detection zone	degeneracy zone
$q = 1/10$	$s \lesssim 24$ ($d \lesssim 46$ AU)	$11 \lesssim s \lesssim 24$ ($21 \lesssim d \lesssim 46$ AU)
$q = 1/5$	$s \lesssim 31$ ($d \lesssim 59$ AU)	$13 \lesssim s \lesssim 31$ ($25 \lesssim d \lesssim 59$ AU)
$q = 1/3$	$s \lesssim 40$ ($d \lesssim 76$ AU)	$16 \lesssim s \lesssim 40$ ($20 \lesssim d \lesssim 76$ AU)
$q = 1/2$	$s \lesssim 50$ ($d \lesssim 95$ AU)	$20 \lesssim s \lesssim 50$ ($38 \lesssim d \lesssim 95$ AU)
$q = 1.0$	$s \lesssim 63$ ($d \lesssim 120$ AU)	$22 \lesssim s \lesssim 63$ ($41 \lesssim d \lesssim 120$ AU)
$q = 2.0$	$s \lesssim 100$ ($d \lesssim 190$ AU)	$25 \lesssim s \lesssim 100$ ($48 \lesssim d \lesssim 190$ AU)

NOTE. — Detection and degeneracy zones of wide-separation binaries. The detection zone represents the range of binary separation where the lensing signature of a companion can be detected. The degeneracy zone indicates the range where the companion can be detected but the characterization of the binary is difficult due to the degeneracy of the binary-lensing parameters. The absolute physical ranges are given assuming a microlensing system with $D_S = 8$ kpc, $D_L = 6$ kpc, and $m_i = 0.3\,M_\odot$.

4. CONCLUSION

By investigating the patterns of central perturbations produced by wide-separation binary companions, we found that the perturbation can be noticed and thus lens binarity can be identified for binaries with considerable separations. However, we also found that perturbations for a significant por-

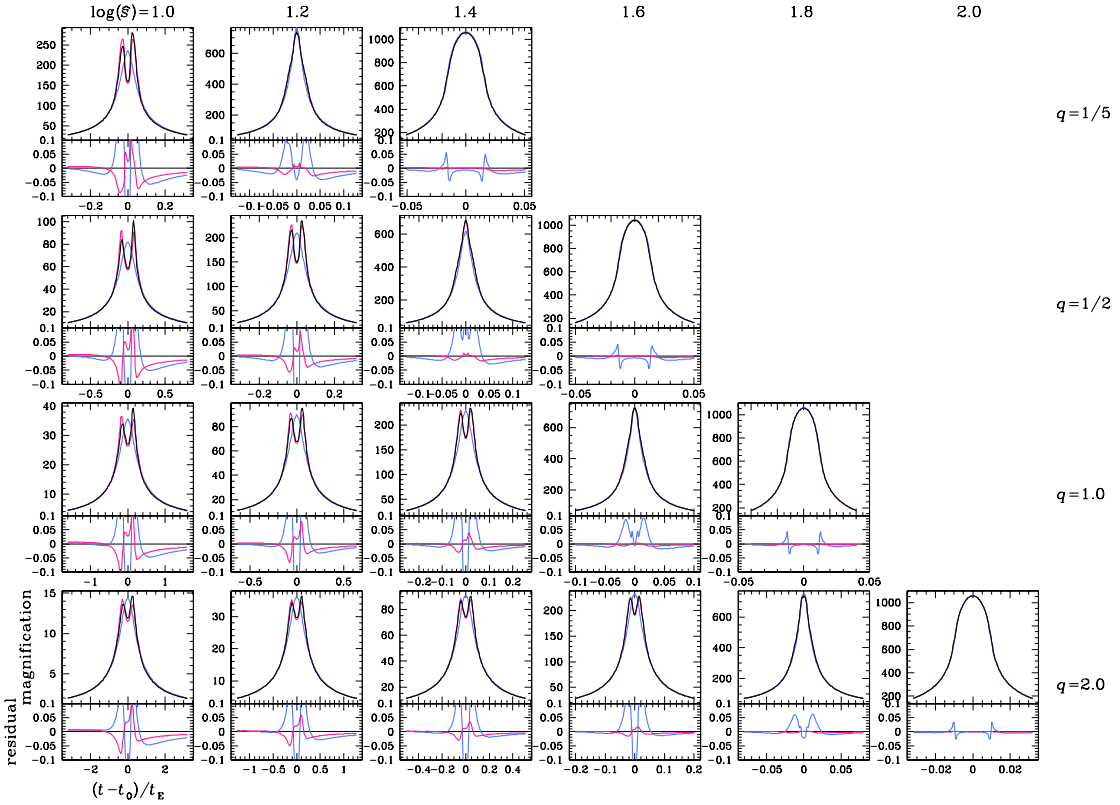

FIG. 3.— Example light curves of high-magnification events caused by wide-separation binaries. The source trajectories responsible for the individual events are marked in the corresponding panels of Fig. 1. In the upper part of each panel, there are three light curves: blue curve for single lensing, red curve for C-R lensing, and black curve for binary lensing. The lower part shows the fractional residuals from the single lensing magnification (blue curve) and the C-R lensing approximation (red curve).

tion of these binaries can be well approximated by the C-R lensing, implying that the individual binary-lensing parameters cannot be separately determined and thus characterization of the binary is difficult. We set the range in the binary-lensing parameter space where this degeneracy occurs. From this, we found that the lens binarity can be noticed up to the separations of ~ 60 times of the Einstein radius corresponding to the mass of each lens of a binary composed of equal mass lenses. Among these binaries, however, we found that the lensing parameters can be determined only for a portion of binaries with separations less than ~ 20 times of the Einstein radius.

C. H. acknowledge support from the Astrophysical Research Center for the Structure and Evolution of the Cosmos (ARCSEC) of the Korea Science and Engineering Foundation (KOSEF) through the Science Research Program (SRC). H.-Y. C. and B-G. P. were supported by the grant (KRF-2006-311-C00072) from Korea Research Foundation.

REFERENCES

Albrow, M. D., et al. 2001, ApJ, 556, L113
Albrow, M. D., et al. 2002, ApJ, 572, 1031
Beaulieu, J. P., et al. 2006, Nature, 439, 437
Bennett, D. P., et al. 2008, ApJ, submitted
Bond, I. A., et al. 2002, MNRAS, 331, L19
Bond, I. A., et al. 2004, ApJ, 606, L155
Chang, K., & Refsdal, S. 1979, 282, 561
Chang, K., & Refsdal, S. 1984, 132, 168
Dominik, M. 1999, A&A, 349, 108
Di Stefano, R., & Mao, S. 1996, ApJ, 457, 93
Dong, S., et al. 2006, ApJ, 642, 842
Dong, S., et al. 2008, ApJ, submitted
Gaudi, B. S., et al. 2008, Science, 319, 927
Gould, A., et al. 2006, ApJ, 644, L37
Gould, A., & Loeb, A. 1992, ApJ, 396, 104
Griest, K., & Safizadeh, N. 1998, ApJ, 500, 37
Han, C., & Gaudi, B. S. 2008, ApJ, in press
Mao, S., & Paczyński, B. 1991, ApJ, 374, L37
Paczyński, B. 1986, ApJ, 304, 1
Udalski, A. 2003, Acta Astron., 53, 291
Udalski, A., et al. 2005, ApJ, 628, L109
Witt, H. J. 1990, A&A, 236, 311